

Neutron Charge Radius: Relativistic Effects and the Foldy Term

W.R.B. de Araújo^a, T. Frederico^a, M. Beyer^b, and H.J. Weber^c

^a *Dep. de Física, Instituto Tecnológico de Aeronáutica, Centro Técnico Aeroespacial,
12.228-900 São José dos Campos, São Paulo, Brazil.*

^b *Fachbereich Physik, Universität Rostock, 18051 Rostock, Germany and*

^c *Dept. of Physics, University of Virginia, Charlottesville, VA 22904, U.S.A.*

(Dated: November 10, 2018)

Abstract

The neutron charge radius is studied within a light-front model with different spin coupling schemes and wave functions. The cancellation of the contributions from the Foldy term and Dirac form factor to the neutron charge form factor is verified for large nucleon sizes and it is independent of the detailed form of quark spin coupling and wave function. For the physical nucleon our results for the contribution of the Dirac form factor to the neutron radius are insensitive to the form of the wave function while they strongly depend on the the quark spin coupling scheme.

PACS numbers: 12.39.-x,13.40.-f,13.40.-Gp,14.20.-c

I. INTRODUCTION

Nowadays, there is a renewed interest in the nucleon electromagnetic form factors due to recent precise experiments[1]. The electroweak static observables are receiving theoretical attention as well, in particular, the neutron charge radius was recently studied with respect to its relativistic origin[2, 3, 4, 5]. From the nonrelativistic point of view the nucleon wave function with SU(6) symmetry implies a zero neutron charge radius and $\mu_p/\mu_n = -m_N/(2m)$ (m_N and m are the masses of the nucleon and constituent quarks, respectively). However, the quark spin-spin interaction that implies the nucleon-delta mass splitting allows the dynamical breaking of the SU(6) symmetry and a nonvanishing neutron charge mean square radius (r_n^2). The flavor identical quarks are pushed out, while the u quark stays around the neutron center, which gives a negative charge mean square radius, in agreement with the observed sign[6].

The experimental value $r_n^2 = -0.113 \pm 0.005 \text{ fm}^2$ [6] is coincidentally near the contribution of the Foldy term ($\frac{3}{2} \frac{\mu_n}{m_n^2} = -0.126 \text{ fm}^2$), and for that reason the contribution of the Dirac form factor (F_{1n}) is quite small, $r_{1n}^2 = 0.013 \pm 0.005 \text{ fm}^2$. The electric and magnetic form factors (Sachs form factors) are given by:

$$\begin{aligned} G_{EN}(q^2) &= F_{1N}(q^2) + \frac{q^2}{4m_N^2} F_{2N}(q^2) , \\ G_{MN}(q^2) &= F_{1N}(q^2) + F_{2N}(q^2) , \end{aligned} \quad (1)$$

where $N = n$ or p , F_{2N} is the Pauli form factor, q^μ is the momentum transfer. The magnetic moment is $\mu_N = G_{MN}(0)$ and the charge mean square radius is $r_N^2 = 6 \frac{dG_{EN}(q^2)}{dq^2} \big|_{q^2=0}$.

The naive physical picture of the spin-spin interaction dominating the negative neutron charge radius is confronted with the fact that the recoil effect from the Foldy term dominates the charge radius. Thus, if one associates the intrinsic charge distribution with F_{1n} , one comes to the wrong conclusion that the spin-spin interaction is not relevant for r_n^2 . The recent work of Isgur[2] clarified this issue, the rest frame charge distribution of the neutron should be associated with the form factor G_{En} and not with F_{1n} . He found that in the the first relativistic correction to the Dirac form factor cancels the Foldy term in a relativistic model of the nucleon within a quark-diquark picture. Consequently, the nonzero value of the neutron charge radius should reflect the intrinsic charge distribution and the detailed quark spin dynamics. In fact, in Ref.[3] it was shown that the different forms of relativistic

quark spin coupling in the nucleon have dramatic effects on the neutron charge mean square radius. The relativistic spin coupling coefficients, which depend on momentum, effectively lead to the breaking of the SU(6) symmetry as discussed in Ref.[4], and to a nonzero neutron charge form factor.

In this work, we focus our attention on the neutron charge mean square radius and our aim is to explore, within a light-front relativistic model[3], the detailed dependence of r_{1n}^2 , obtained from F_{1n} , on the nucleon size that is parametrized by the proton charge radius (r_p). The proton charge radius controls the relativistic or nonrelativistic nature of the constituent three-quark system. For $r_p \gg m^{-1}$, the inverse constituent quark mass, the nucleon approaches a nonrelativistic system of quarks. On the other hand for $r_p \sim m^{-1} \sim 1$ fm (the real nucleon size and constituent mass scales), the three-quark system demands a relativistic description of the internal quark motion. The parameters of the light-front model are adjusted to different nucleon sizes, with several forms of momentum component of the wave function and quark spin coupling schemes. By changing the parameters we are able to shift smoothly from relativistic to nonrelativistic regimes. In the nonrelativistic regime we show quite generally the cancellation between r_{1n}^2 and the Foldy term contribution to the neutron charge radius, while at the physical nucleon scale the value of r_{1n}^2 is strongly dependent on the choice of quark spin coupling scheme.

Following our previous work[3], where we have studied the nucleon electroweak form factors using different forms of relativistic spin coupling between the constituent quarks to form the nucleon, we use an effective Lagrangian to describe the coupling of the quark spin. The form factor calculation keeps close contact with covariant field theory. The starting point is the impulse approximation for the nucleon virtual photon absorption amplitude, which is projected on the three-dimensional null-plane hypersurface, $x^+ = x^0 + x^3 = 0$, (see, e.g., Ref. [7]). The three-dimensional reduction is done by integrating over the individual light-front energies ($k^- = k^0 - k^3$) in the two-loop momentum integrations of the impulse approximation. The relative light-front time between the particles is eliminated in favor of the global time propagation[8]. Then, the momentum component of the nucleon light-front wave function is introduced into the remaining form of the two-loop momentum three-dimensional integrations which define the matrix elements of the electroweak current [3, 9, 10]. In general, the vertex function depends on the quark momentum variables $x_i, \vec{k}_{i\perp}$ and is chosen to be totally symmetric. We make the common assumption that the vertex function

depend on the free three-quark light-cone energy, M_0^2 (Eq. 9), which is the simplest totally symmetric scalar function of the quark momentum variables.

The effective Lagrangian for the $N - q$ coupling is written as[3],

$$\mathcal{L}_{N-3q} = \alpha m_N \epsilon^{lmn} \bar{\Psi}_{(l)} i\tau_2 \gamma_5 \Psi_{(m)}^C \bar{\Psi}_{(n)} \Psi_N + (1 - \alpha) \epsilon^{lmn} \bar{\Psi}_{(l)} i\tau_2 \gamma_\mu \gamma_5 \Psi_{(m)}^C \bar{\Psi}_{(n)} i\partial^\mu \Psi_N + h.c. \quad (2)$$

where τ_2 is the isospin matrix, the color indices are $\{l, m, n\}$ and ϵ^{lmn} is the totally anti-symmetric symbol. The conjugate quark field is $\Psi^C = C \bar{\Psi}^\top$, where $C = i\gamma^2\gamma^0$ is the charge conjugation matrix; α is a parameter to choose the spin coupling parameterization.

In Ref. [3] we have tested different spin couplings for the nucleon in a calculation of nucleon electroweak form factors. We have found that the neutron charge form factor constrains the relativistic quark spin coupling schemes. The neutron data below momentum transfers of 1 GeV/c suggested that the scalar pair ($\alpha = 1$) in the effective Lagrangian is preferred. In that study, Gaussian and power law momentum components of the wave functions were used. Here we enlarge the set of momentum components of the wave functions to allow a wide variation of parameters, to shift from relativistic to nonrelativistic regimes.

This work is organized as follows. In section II, it is given a brief description of the macroscopic and microscopic forms of the nucleon electromagnetic current appropriate for the light-front calculations. In section III, we present the numerical analysis of the static nucleon observables for different model assumptions. A summary and conclusion is presented in section IV.

II. NUCLEON ELECTROMAGNETIC CURRENT

A. Macroscopic matrix elements

The electromagnetic form factors are extracted from the plus component of the current for momentum transfers satisfying the Drell-Yan condition $q^+ = q^0 + q^3 = 0$. The contribution of the Z-diagram is minimized in a Drell-Yan reference frame while the wave function contribution to the current is maximized[7, 9, 10, 11, 12]. In particular, the Breit-frame is chosen, with four momentum transfer $q = (0, \vec{q}_\perp, 0)$, such that $(q^+ = 0)$ and $\vec{q}_\perp = (q^1, q^2)$. The nucleon momentum in the initial state is $p = (\sqrt{\frac{q_1^2}{4} + m_N^2}, -\frac{\vec{q}_\perp}{2}, 0)$ and in the final state is given by $p' = (\sqrt{\frac{q_1^2}{4} + m_N^2}, \frac{\vec{q}_\perp}{2}, 0)$.

The macroscopic matrix element of the nucleon electromagnetic current $J_N^+(q^2)$ in the Breit-frame and in the light-front spinor basis is given by:

$$\begin{aligned}\langle s' | J_N^+(q^2) | s \rangle &= \bar{u}(p', s') \left(F_{1N}(q^2) \gamma^+ + i \frac{\sigma^{+\mu} q_\mu}{2m_N} F_{2N}(q^2) \right) u(p, s) \\ &= \frac{p^+}{m_N} \langle s' | F_{1N}(q^2) + i \frac{F_{2N}(q^2)}{2m_N} \vec{q}_\perp \cdot (\vec{\sigma} \times \vec{n}) | s \rangle ,\end{aligned}\quad (3)$$

where F_{1N} and F_{2N} are the Dirac and Pauli form factors, respectively, while \vec{n} is the unit vector along the z-direction.

The light-front spinors are defined as:

$$u(p, s) = \frac{\not{p} + m_N}{2\sqrt{p^+ m_N}} \gamma^+ \gamma^0 \begin{pmatrix} \chi_s^{\text{Pauli}} \\ 0 \end{pmatrix} , \quad (4)$$

and the Dirac spinor of the instant form is given by

$$u_D(p, s) = \frac{\not{p} + m_N}{\sqrt{2m(p^0 + m)}} \begin{pmatrix} \chi_s^{\text{Pauli}} \\ 0 \end{pmatrix} \quad (5)$$

which carries the subscript D . The Melosh rotation is the unitary transformation between the light-front and instant form spinors, which is given by:

$$[R_M(p)]_{s's} = \langle s' | \frac{\not{p} + m - i\vec{\sigma} \cdot (\vec{n} \times \vec{p})}{\sqrt{(p^+ + m)^2 + p_\perp^2}} | s \rangle = \bar{u}_D(p, s') u(p, s) . \quad (6)$$

B. Microscopic matrix elements

The microscopic matrix elements of the nucleon electromagnetic current is derived from the effective Lagrangian, Eq.(2), within the light-front impulse approximation which is represented by the two-loop diagrams of figure 1[3]. The complete antisymmetrization of the quark states implies that the matrix element of the current is composed by four topologically distinct diagrams depicted in the figure. The matrix elements of the electromagnetic current are calculated considering only the process on quark 3, due to the symmetrization of the microscopic matrix element after the factorization of the color degree of freedom. The four distinct current operators $J_{\beta N}^+$, $\beta = a, b, c, d$, are constructed from the Feynman diagrams of figure 1a to 1d, respectively[3].

The microscopic operator of the nucleon electromagnetic current, J_N^+ , is the sum of each amplitude represented by the diagrams (1a) to (1d):

$$J_N^+(q^2) = J_{aN}^+(q^2) + 4J_{bN}^+(q^2) + 2J_{cN}^+(q^2) + 2J_{dN}^+(q^2) ; \quad (7)$$

where the weighting factors comes from the identity of quarks 1 and 2, and another factor 2 multiplying J_{bN}^+ comes from the exchange of the pairs in the initial and final nucleons, which gives the same matrix element as a consequence of time reversal and parity transformation properties.

The light-front momentum are defined as $k^+ = k^0 + k^3$, $k^- = k^0 - k^3$, $k_\perp = (k^1, k^2)$. In each term of the nucleon plus component of the current, from J_{aN}^+ to J_{dN}^+ , the quark momenta are on- k^- -shell. The total plus and transverse momentum components of the intermediate states satisfy conservation laws. Thus, the components of the momentum k_1^+ and k_2^+ are bounded, such that $0 < k_1^+ < p^+$ and $0 < k_2^+ < p^+ - k_1^+$ [13].

The two-loop Feynman diagram of figure 1a corresponds to

$$\begin{aligned} \langle s' | J_{aN}^+(q^2) | s \rangle = & 2p^{+2} \langle N | \hat{Q}_q | N \rangle \int \frac{d^2 k_{1\perp} dk_1^+ d^2 k_{2\perp} dk_2^+}{k_1^+ k_2^+ k_3^+} \theta(p^+ - k_1^+) \theta(p^+ - k_1^+ - k_2^+) \\ & \text{Tr} [(\not{k}_2 + m) (\alpha m_N + (1 - \alpha) \not{p}) (\not{k}_1 + m) (\alpha m_N + (1 - \alpha) \not{p}')] \\ & \bar{u}(p', s') (\not{k}_3' + m) \gamma^+ (\not{k}_3 + m) u(p, s) \Psi(M_0'^2) \Psi(M_0^2), \end{aligned} \quad (8)$$

where $k_1^2 = m^2$ and $k_2^2 = m^2$. The momentum component of the wave function is $\Psi(M_0^2)$ and the free three-quark squared mass is defined by:

$$M_0^2 = p^+ \left(\frac{k_{1\perp}^2 + m^2}{k_1^+} + \frac{k_{2\perp}^2 + m^2}{k_2^+} + \frac{k_{3\perp}^2 + m^2}{k_3^+} \right) - p_\perp^2, \quad (9)$$

and $M_0'^2 = M_0^2(k_3 \rightarrow k_3', \vec{p}_\perp \rightarrow \vec{p}_\perp')$. The electromagnetic quark current operator is $\bar{\Psi} \hat{Q}_q \gamma^\mu \Psi$, with \hat{Q}_q the charge operator and Ψ the quark field.

The other terms of the nucleon current, represented in figures 1b to 1d, are written below:

$$\begin{aligned} \langle s' | J_{bN}^+(q^2) | s \rangle = & p^{+2} \langle N | \hat{Q}_q | N \rangle \int \frac{d^2 k_{1\perp} dk_1^+ d^2 k_{2\perp} dk_2^+}{k_1^+ k_2^+ k_3^+} \theta(p^+ - k_1^+) \theta(p^+ - k_1^+ - k_2^+) \\ & \bar{u}(p', s') (\not{k}_3' + m) \gamma^+ (\not{k}_3 + m) (\alpha m_N + (1 - \alpha) \not{p}) (\not{k}_1 + m) \\ & \times (\alpha m_N + (1 - \alpha) \not{p}') (\not{k}_2 + m) u(p, s) \Psi(M_0'^2) \Psi(M_0^2), \end{aligned} \quad (10)$$

$$\begin{aligned} \langle s' | J_{cN}^+(q^2) | s \rangle = & p^{+2} \langle N | \tau_2 \hat{Q}_q \tau_2 | N \rangle \int \frac{d^2 k_{1\perp} dk_1^+ d^2 k_{2\perp} dk_2^+}{k_1^+ k_2^+ k_3^+} \theta(p^+ - k_1^+) \theta(p^+ - k_1^+ - k_2^+) \\ & \bar{u}(p', s') (\not{k}_1 + m) (\alpha m_N + (1 - \alpha) \not{p}) (\not{k}_3 + m) \gamma^+ (\not{k}_3' + m) \\ & \times (\alpha m_N + (1 - \alpha) \not{p}') (\not{k}_2 + m) u(p, s) \Psi(M_0'^2) \Psi(M_0^2), \end{aligned} \quad (11)$$

$$\begin{aligned} \langle s' | J_{dN}^+(q^2) | s \rangle = & p^{+2} \text{Tr}[\hat{Q}_q] \int \frac{d^2 k_{1\perp} dk_1^+ d^2 k_{2\perp} dk_2^+}{k_1^+ k_2^+ k_3^+} \theta(p^+ - k_1^+) \theta(p^+ - k_1^+ - k_2^+) \\ & \text{Tr} [(\alpha m_N + (1 - \alpha) \not{p}') (\not{k}_3' + m) \gamma^+ (\not{k}_3 + m) (\alpha m_N + (1 - \alpha) \not{p}) (\not{k}_1 + m)] \\ & \bar{u}(p', s') (\not{k}_2 + m) u(p, s) \Psi(M_0'^2) \Psi(M_0^2). \end{aligned} \quad (12)$$

In our study, for simplicity and as is explicit in Eqs.(8) to (12), the same momentum wave function is chosen for both $N - q$ couplings. The momentum part of the wave function in the microscopic matrix element of the current is chosen from different models as we will show in the next section.

III. RESULTS FOR STATIC NEUTRON OBSERVABLES

In this section we present our theoretical results for static nucleon charge square radius assuming the dominance of the lowest light-front Fock state component in the nucleon wave function corresponding to three constituent quarks. By itself this is a strong constraint on the static observables and essentially the results are mostly dependent on the constituent quark mass and scale with proton charge radius, as it will be shown. We use a constituent quark mass value of $m = 0.22 \text{ GeV}$ from Refs.[3, 15].

Within the above assumptions, we show the effects of different relativistic spin couplings and momentum wave functions of constituent quarks for the neutron and proton charge square radius. The key point in our discussion is the detailed dependence of

$$r_{1n}^2 = 6 \frac{d}{dq^2} F_{1n}(q^2)$$

on the nucleon size, parameterized by the proton charge radius (r_p), which controls the relativistic or nonrelativistic nature of the constituent three-quark system. The Foldy term contribution to the neutron charge square radius is

$$r_{2n}^2 = \frac{3}{2} \frac{\mu_n}{m_N^2} ,$$

and the square of the neutron charge radius is the sum of both contributions, i.e., $r_n^2 = r_{1n}^2 + r_{2n}^2$.

The parameters of the light-front model are changed to allow different nucleon sizes for different forms of momentum component of the wave function and quark spin coupling schemes. By modifying the parameters a smooth shift from relativistic to nonrelativistic regimes is obtained. The nonrelativistic regime of the constituent quark system is characterized by $r_p^2 > 1 \text{ fm}^2$ (about the inverse of the constituent quark mass squared), and the relativistic regime by $r_p^2 < 1 \text{ fm}^2$ (the real nucleon size and constituent mass scales).

The correlations between the neutron charge square radius with magnetic moment and proton charge square radius are investigated with a different momentum part of the nucleon

light-front wave function for each quark spin coupling scheme. Among the observables, the neutron charge radius plays a special role; its correlation with the magnetic moment depends on the quark spin coupling scheme[3].

A. Model wave functions

The matrix elements of the microscopic nucleon plus component of the current, Eqs.(8) to (12), are evaluated for different $N - q$ spin couplings and momentum part of the wave function. The different models of the momentum component of the wave function corresponds to the choices of the harmonic and power-law forms [11, 14],

$$\Psi_{\text{HO}} = N_{\text{HO}} \exp(-M_0^2/2\beta^2) \quad , \quad \Psi_{\text{Power}} = N_{\text{Power}} (1 + M_0^2/\beta^2)^{-p} \quad (13)$$

and modified harmonic and power-law wave functions

$$\Psi'_{\text{HO}} = N'_{\text{HO}} \frac{\exp(-M_0^2/2\beta^2)}{\beta_1^2 - M_0^2} \quad , \quad \Psi'_{\text{Power}} = N'_{\text{Power}} \frac{(1 + M_0^2/\beta^2)^{-p}}{\beta_1^2 - M_0^2} \quad (14)$$

The normalization is determined by the proton charge. The width parameter is β . The free mass of the three-quark system satisfies $M_0 > 3m$ and β_1 has to satisfy the constraint $\beta_1 < 3m$ to avoid scattering poles in the bound state wave function of Eq.(14). This property is consistent with color confinement which prevents scattering states of three quarks to be relevant.

The wave function models of Eq. (14) are inspired in the general form of the lowest Fock-state component of the nucleon wave function in QCD light-front field theory where the complete wave function is an eigenstate of the complete mass operator equation[11, 16]. The lowest Fock state component of the hadron wave function satisfies an effective mass operator equation for constituent quark degrees of freedom, in which the effective interaction contains in principle all the complexity of QCD [11, 16]. The general form of lowest Fock component in terms of the constituent quark degrees of freedom has the term $(\beta_1^2 - M_0^2)^{-1}$, where β_1 plays the role of the mass of a bound system. Here, we use the models for the wave function from Eq. (14) just to enlarge our possible choices of momentum components of the wave function, while still keeping connection with the basic QCD theory.

From general QCD perturbative arguments a power-law fall-off with $p = 3.5$ is predicted for Ψ_{Power} [11, 14]. The correlations between static electroweak observables are not sensitive to p as long as $p > 2$ [3, 14] and we choose for our calculations $p = 3$ in both Ψ_{Power} and Ψ'_{Power} . For large virtualities $\Psi_{\text{Power}} \sim M_0^{-2p}$ and $\Psi'_{\text{Power}} \sim M_0^{-2(p+1)}$, with $p = 3$, which is above and below the QCD power fall-off, respectively. As we are going to show below these different assumptions for the wave function have only little effect in the correlations between the static observables.

B. Numerical Results

In Figs. 2 to 5 we show results for the correlations between static neutron charge square radius, magnetic moment and proton radius. Our calculations are done for different spin couplings of quarks, i.e. $\alpha = 0, 1/2, 1$ in the effective Lagrangian of Eq.(2), and momentum wave functions of a harmonic oscillator (HO) (Gaussian) and a power-law (Power) form ($p = 3$) from Eq. (13) and the modified forms from Eq. (14).

The correlation of the static observables is found by variation of the β and β_1 parameters. In the Gaussian wave function of Eq.(13) two limits are noteworthy, $\beta \rightarrow 0$ leads to an infinite size of the nucleon corresponding to the nonrelativistic limit and $\beta \rightarrow \infty$ is the zero radius limit corresponding to the strong relativistic limit. In the power-law wave functions for $\beta \rightarrow \infty$ the relativistic limit is approached. However in this case of $\beta \rightarrow 0$ one does not approach the nonrelativistic limit because the typical momentum scale of the wave function is the quark mass and not zero. The modified Gaussian and power-law wave function of Eq. (14) are much more flexible, because the nonrelativistic limit can be approached by taking $\beta_1 \rightarrow 3m$, which corresponds to zero binding energy, and the quark system swells to infinity. Taking β going to infinity in the Gaussian and in the modified Gaussian models, the nucleon tends to zero size, and to the extreme relativistic regime. In our results we explore a wide range of values of β and β_1 .

In Figure 2 results are shown for the neutron charge radius as a function of the neutron magnetic moment for $\alpha = 0, 1/2$, and 1 as well as HO, Power, modified HO and Power momentum wave functions. The results are quite insensitive to the different shapes of the momentum wave functions, however strongly dependent on the quark spin coupling as we have already found in Ref.[3]. The present extension to several different forms of

wave function confirms the previous findings, and moreover the confining or nonconfining behavior of the wave function is not important for the neutron radius as long as the magnetic moment is fitted. The nonconfining feature of the wave function does not change our previous conclusion, i.e., the experimental data for the neutron charge radius favors the scalar coupling between the quark-pair, while the gradient spin coupling ($\alpha = 0$) completely disagrees with the experimental value.

As our main point is to study the neutron radius as a function of the nucleon size, parameterized by the proton charge radius, next we show in Figure 3 the neutron charge square radius as a function of the proton charge square radius, for the same set of calculations presented in Figure 2. The different models of quark spin couplings (for α equal to 0, 1/2 and 1) are shown in Figure 3 and represent a systematic behavior that once again is quite independent of the form of the momentum component of the wave function. For the chosen constituent mass ($m = 0.22$ GeV) the experimental points from [17, 18, 19] data are within the width for the theoretical results for the scalar coupling. The results for the modified Gaussian and power-law wave functions are obtained by changing either β or β_1 in Eq.(14), which leads to a small spread of the results seen in the figure.

The functional dependence of the individual contributions r_{1n}^2 and r_{2n}^2 to the neutron charge square radius with proton charge square radius is shown in Figure 4. The relativistic and nonrelativistic regimes are identified in the figure. For the proton charge square radius below 3 fm^2 , we observe the intrinsic relativistic behavior of the quark motion through the wide separation of the results for r_{1n}^2 obtained for different quark spin coupling schemes. The nonrelativistic regime is seen for r_p^2 above 3 fm^2 where the calculations tend to be flat and with magnitude which cancels to some extent the contribution of Foldy term, r_{2n}^2 . At the physical nucleon size scale $r_p \sim 0.8 \text{ fm}$, the quark motion is quite relativistic, where r_{1n}^2 has a sensitive dependence on the spin couplings, i.e. α . The result for r_{1n}^2 is about zero for the scalar coupling which implies in this case the dominance of the Foldy term in the neutron charge radius. The dependence on the details of the momentum component of the wave function is quite small.

To be complete, we present in Figure 5 the function defined by $r_n^2(r_p^2)$ over the same range of proton sizes as in Figure 4. The results for the neutron square charge radius show a smooth trend in all models and spin coupling schemes from the physical scale (relativistic regime) towards the nonrelativistic regime. The cancellation of the Foldy term in the nonrelativistic

regime leads to the small values of r_n^2 for all models investigated despite the differences in the quark spin coupling schemes and wave functions. We show the cancellation between r_{1n}^2 and the Foldy term contribution, r_{2n}^2 to the neutron charge radius in the nonrelativistic regime for the particular coupling of Eq. (2), while at the physical nucleon scale the value of r_{1n}^2 is strongly dependent on the choice of quark spin coupling scheme.

IV. SUMMARY AND CONCLUSION

In this work we have studied in detail the effect of the nucleon size scale in the individual contribution of the Dirac form factor to the neutron charge square radius, using a relativistic light-front model with constituent quarks. The model is constructed with different relativistic spin coupling schemes and wave functions. The wave function parameters were adjusted to different nucleon sizes, parameterized by the proton charge radius, which allowed us to investigate the cancellation between the contributions from the Foldy term (r_{2n}^2) and Dirac form factor (r_{1n}^2) in the neutron charge square radius that occurs in nonrelativistic regimes[2].

First we extend the previous analysis of the neutron static observables [3], using more general forms of the momentum component of the wave function, which have a nonconfining tail and we find a model independent correlation of the Foldy term and r_{1n}^2 with the proton charge radius for each spin coupling scheme. The existence of the model independent correlation of r_{2n}^2 and r_{1n}^2 with the proton charge radius allowed the study of the nucleon size scale effects on a physical ground.

Our calculations show that the cancellation between r_{1n}^2 and the Foldy term contribution, r_{2n}^2 to the neutron charge radius happens indeed to a large extent in the nonrelativistic regime, independent of the detailed form of quark spin coupling scheme and wave function. The nonrelativistic regime is seen in our calculations for the square of the proton charge radius above 3 fm^2 where the contributions of the Dirac form factor and Foldy term to the neutron charge square radius tend to cancel. At the physical nucleon scale the value of r_{1n}^2 is strongly dependent on the choice of quark spin coupling scheme, a consequence of the intrinsic relativistic nature of the constituent quark motion inside the nucleon.

Acknowledgments: WRBA thanks FAPESP (Fundação de Amparo à Pesquisa do Estado de São Paulo) for financial support and LCCA/USP for providing computational facil-

ties. TF thanks CNPq (Conselho Nacional de Pesquisas) and FAPESP.

- [1] M.K. Jones et al.[Jefferson Lab Hall A collaboration], *Phys. Rev. Lett.* **84**, 1398 (2000).
- [2] N. Isgur, *Phys. Rev. Lett.* **83**, 272 (1999).
- [3] W.R.B. de Araújo, E.F. Suisso, T.Frederico, M. Beyer and H.J. Weber, *Phys. Lett.* **B478**, 86 (2000); E.F. Suisso, W.R.B. de Araújo, T.Frederico, M.Beyer and H.J. Weber, *Nucl. Phys.* **A694**, 351 (2001).
- [4] F. Cardarelli and S. Simula, *Phys. Rev.* **C62**, 065201 (2000).
- [5] V. A. Karmanov, *Nucl. Phys.* **A699**, 148 (2002).
- [6] S. Kopecky et al., *Phys. Rev. Lett.* **74**, 2427 (1995).
- [7] J. Carbonell, B. Desplanques, V. Karmanov and J.-F. Mathiot, *Phys. Reports* **300**, 215 (1998), and references therein.
- [8] J. H. O. Sales, T. Frederico, B. V. Carlson and P. U. Sauer, *Phys. Rev.* **C61**, 044003 (2000); *Phys. Rev.* **C63**, 064003 (2001).
- [9] T. Frederico and G.A. Miller, *Phys. Rev.* **D45**, 4207 (1992).
- [10] J.P.B.C de Melo, H.W. Naus and T. Frederico, *Phys. Rev.* **C59**, 2278 (1999).
- [11] S.J. Brodsky, H.-C. Pauli and S.S. Pinsky, *Phys. Rep.* **301**, 299 (1998).
- [12] B.L.G. Bakker, H.-M. Choi and C.-R. Ji, *Phys. Rev.* **D63**, 074014 (2001).
- [13] J.P.B.C. de Melo and T. Frederico, *Phys. Rev.* **C55**, 2043 (1997).
- [14] S.J. Brodsky and F. Schlumpf, *Phys. Lett.* **B329**, 111 (1994); *Prog. Part. Nucl. Phys.* **34**, 69 (1995).
- [15] F. Cardarelli, E. Pace, G. Salme and S. Simula, *Phys. Lett.* **B357**, 267 (1995); *Few Body Syst. Suppl.* **8**, 345 (1995); F. Cardarelli and S. Simula, *Phys. Lett.* **B467**, 1 (1999).
- [16] H.-C. Pauli, *Eur. Phys. J.* **C7**, 289 (1998); “DLCQ and the effective interactions in hadrons” in: *New Directions in Quantum Chromodynamics*, C.-R. Ji and D.P. Min, Editors, American Institute of Physics, 1999, p.80-139.
- [17] S.J. Brodsky and J.R. Primack, *Ann. Phys. (N.Y.)* **52**, 315 (1969).
- [18] J.J. Murphy II, Y.M. Shin, and D.M. Skopik, *Phys. Rev.* **C9**, 3125 (1974).
- [19] R. Rosenfelder, *Phys. Lett.* **B479**, 381 (2000).

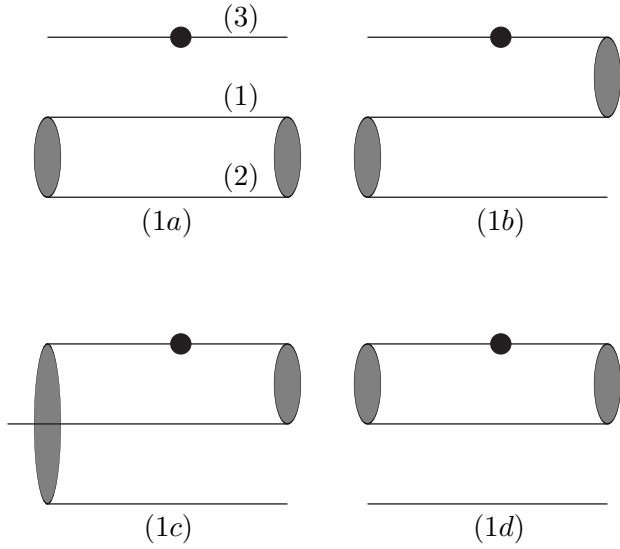


FIG. 1: Light-cone time-ordered diagrams for the nucleon electromagnetic current. The gray blob represents the spin invariant for the coupled quark pair in the effective Lagrangian, Eq.(2). The black circle in the fermion line represents the action of the current operator on the quark. Diagram (1a) represents J_{aN}^+ , Eq.(8). Diagram (1b) represents J_{bN}^+ , Eq.(10). Diagram (1c) represents J_{cN}^+ , Eq.(11). Diagram (1d) represents J_{dN}^+ , Eq.(12).

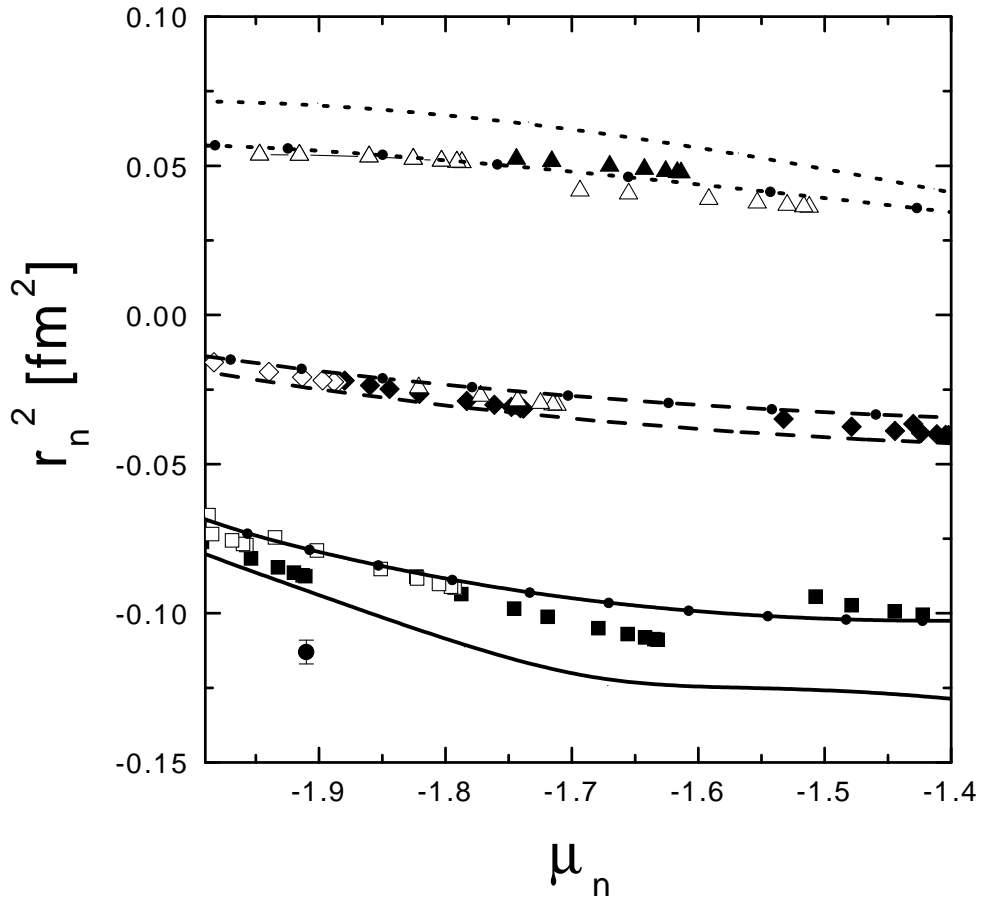


FIG. 2: Neutron charge square radius as a function of the neutron magnetic moment. Results for the Gaussian wave function with α equal to 1 (solid line), 1/2 (dashed line) and 0 (short-dashed line). Results for the power-law wave function with α equal to 1 (solid line with dots), 1/2 (dashed line with dots) and 0 (short-dashed line with dots). Results for modified Gaussian wave function with α equal to 1 (full square), 1/2 (full diamond) and 0 (full triangle). Results for modified power-law wave function with α equal to 1 (open square), 1/2 (open diamond) and 0 (open triangle). Experimental data from Ref.[6].

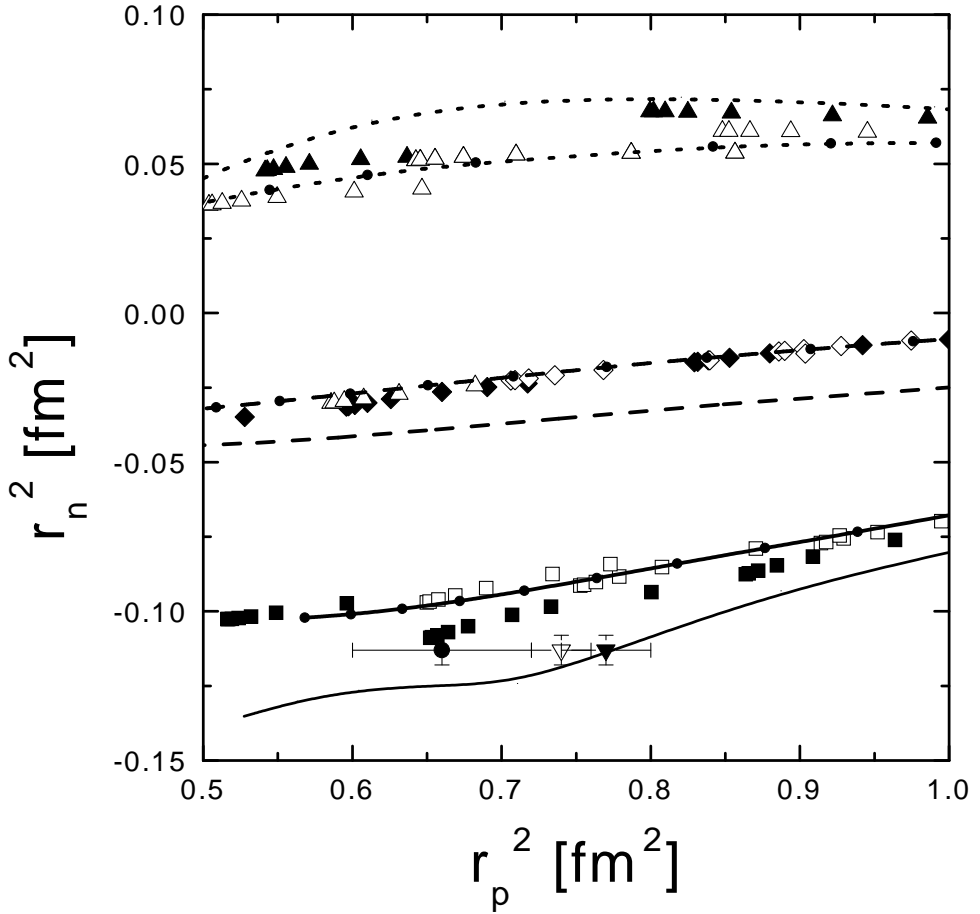


FIG. 3: Neutron charge square radius as a function of the proton charge square radius. Theoretical results labeled as in figure 2. The experimental data points come from the measured value of the neutron charge square radius[6], and from the experimental values of the proton charge square radius from Refs. [17], [18] and [19], which are represented by the full circle, open inverse triangle and full inverse triangle, respectively.

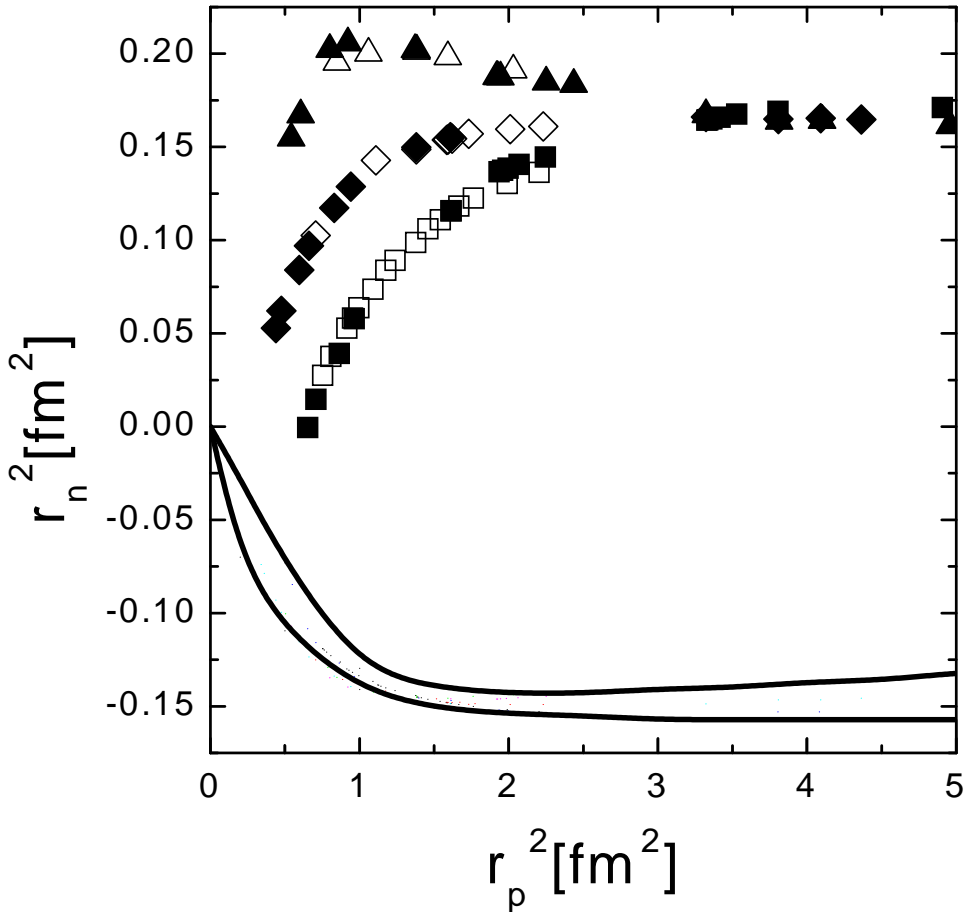


FIG. 4: Individual contributions to the neutron charge radius related to the Dirac form factor $F_{1n}(q^2)$ (r_{1n}^2) and from $F_{2n}(q^2)$ (r_{2n}^2) as a function of the proton charge square radius. Theoretical results (squares, diamonds, triangles) for r_{1n}^2 labeled as in figure 2. Theoretical results for the Foldy term, r_{2n}^2 , are bounded by the thick solid lines.

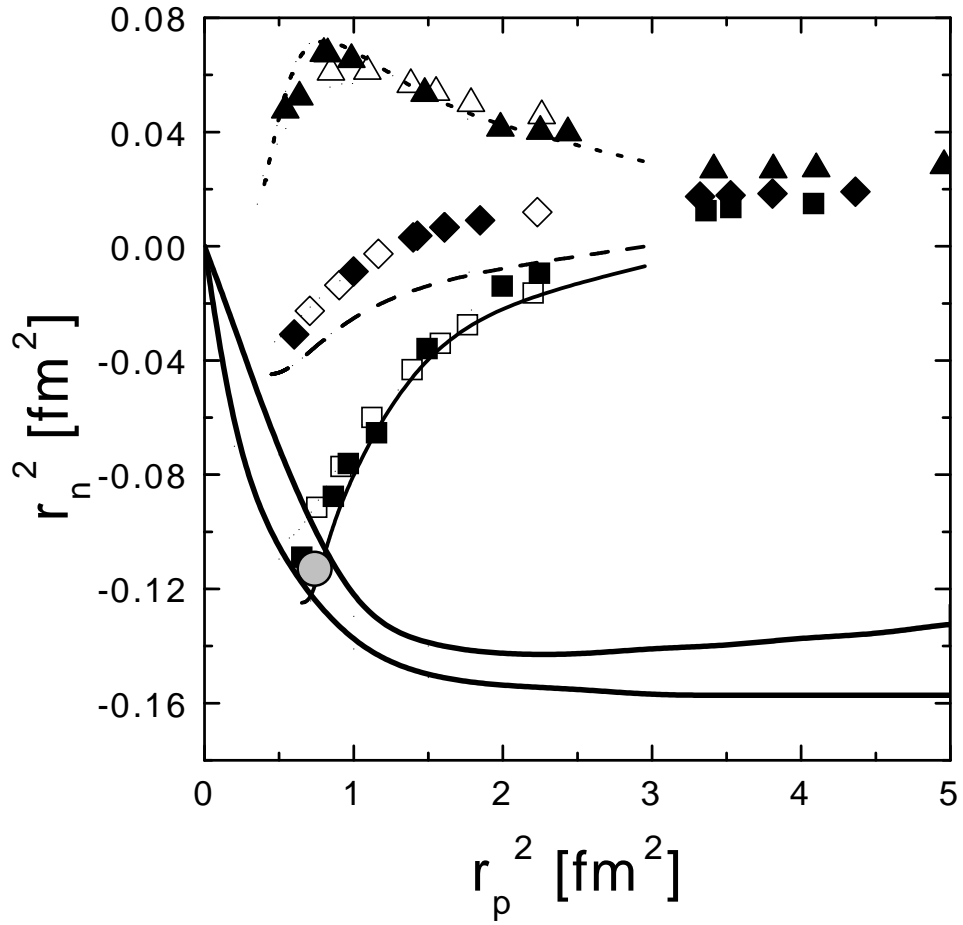


FIG. 5: Neutron charge square radius and r_{2n}^2 as a function of the proton charge square radius. Theoretical results for the Gaussian, modified Gaussian and modified power-law wave functions with α equal to 1, 1/2 and 0, labeled as in figure 2. Experimental points included in gray circle [17, 18, 19].